Vol 17 No 5, May 2008
1674-1056/2008/17(05)/1809-08

Chinese Physics B

© 2008 Chin. Phys. Soc.
and IOP Publishing Ltd

Numerical simulation of end-pumped CW Nd^{3+}:$GdVO_4$ laser at 1063 nm*

Zu Ning-Ning(祖宁宁), Sun Gui-Juan(孙桂娟), and Dai Zhen-Wen(戴振文)†

Department of Physics, Jilin University, Changchun 130023, China
Key Laboratory of Coherent Light, Atomic and Molecular Spectroscopy, Ministry of Education, Changchun 130023, China

(Received 18 August 2007; revised manuscript received 17 September 2007)

A theoretical model to simulate an end-pumped CW Nd^{3+}:$GdVO_4$ laser at 1063 nm is presented. Its essence is to use the propagation equations to demonstrate the spatial evolutions of the pump and the laser powers in the cavity, hence it is applicable to both low and high gain lasers. The simulation results obtained by this model are in good agreement with the experimental observations reported in the literature for a Ti:sapphire-pumped Nd^{3+}:$GdVO_4$ laser. Moreover, some parameters, such as the reflectivity of output coupler, the spot size of laser beam and the crystal length, are discussed with a view to optimizing the laser performance.

Keywords: end-pumped, Nd^{3+}:$GdVO_4$, 1063 nm laser
PACC: 4255, 4255B, 4260D, 4270

1. Introduction

Nd^{3+}:$GdVO_4$ laser crystal with a space group $D_{4h}^{19} - I4_1$, and, a isomorph of Nd^{3+}:YVO_4, were first introduced by Russian and German scientists in 1992.[1] Both Nd^{3+}:$GdVO_4$ and Nd^{3+}:YVO_4 crystals have a higher absorption coefficient at 808 nm and larger emission cross section than a Nd^{3+}:YAG crystal,[2,3] but the advantage of Nd^{3+}:$GdVO_4$ crystal is that its thermal conductivity is twice higher than that of Nd^{3+}:YVO_4 crystal, 11.1W·m^{-1}·K^{-1} in ⟨110⟩ direction,[4] which is comparable with that of a Nd^{3+}:YAG crystal. An additional advantage of Nd^{3+}:$GdVO_4$ is the accidental degeneration of the two Stark components of emitting level $^4F_{3/2}$, and thus all the population of this level can serve for laser emission.[1−3] Such unique spectroscopic and thermal properties make Nd^{3+}:$GdVO_4$ crystal a promising substitute for Nd^{3+}:YVO_4 and Nd^{3+}:YAG in end-pumped compact solid-state lasers.

It is well known that Nd^{3+} ion has multiple allowed transitions from the metastable level $^4F_{3/2}$ to Stark sublevels of the lower-lying energy levels $^4I_{13/2}$, $^4I_{11/2}$ and $^4I_{9/2}$,[5,6] leading to potential laser radiations around 1341, 1063, and 912 nm in Nd^{3+}:$GdVO_4$ crystal, respectively. Because the 1063-nm laser operates in a four-level system and the laser emission cross section at this wavelength is larger than at the other wavelengths, the laser at 1063 nm is easy to obtain. Over the last few years, remarkable progresses have been made in developing highly-efficient end-pumped CW Nd^{3+}:$GdVO_4$ lasers at 1063nm.[7−11]

In this paper we present a complete numerical simulation for the performance of an end-pumped CW Nd^{3+}:$GdVO_4$ laser at 1063 nm. The simulation results are compared with the published experimental results, and on this basis, we discuss the parameters to optimize the laser performance. A analytical model for end-pumped CW Nd-doped lasers has been proposed.[12,13] In the model, by using the space-dependent rate equations and spatial distribution functions of the pump energy and the laser photons, many important laser performance parameters, such as the threshold and the slope efficiency, can be given in the analytical form; but the laser power in the cavity is regarded as a constant, which is only appropriate to describing the behaviours of low gain lasers. Compared with their model, our model adopts the method of combining a rate equation and propagation equation[14,15] to describe the laser performance and use point-by-point and iteration method to numerically solve the equation group.[16] Because the propagation equations can demonstrate the spa-

*Project supported by the National Natural Science Foundation of China (Grant No 10104009).
†Corresponding author. E-mail: dai@jlu.edu.cn

tial evolutions of the pump and the laser powers in the cavity, our model is more accurate to describe the behaviours of high gain lasers. For example, when the incident pump power is high as 10W, the calculated laser power has a gain of 11.4% in the cavity. The aim of this paper is to obtain a better understanding of the kinetic behaviours of this kind of laser and then to provide significant guidelines for designing highly-efficient end-pumped CW Nd^{3+}:$GdVO_4$ lasers.

2. Theory

A general energy-level scheme for the model described here is shown in Fig.1. Two (kinds of) pumping schemes, i.e., direct pumping at 879 nm and indirect pumping at 808 nm can be used to pump Nd^{3+} ions into $^4F_{3/2}$ level, respectively. The 1063-nm Nd^{3+}:$GdVO_4$ laser operates through the $^4F_{3/2} \rightarrow {}^4I_{11/2}$ transition.

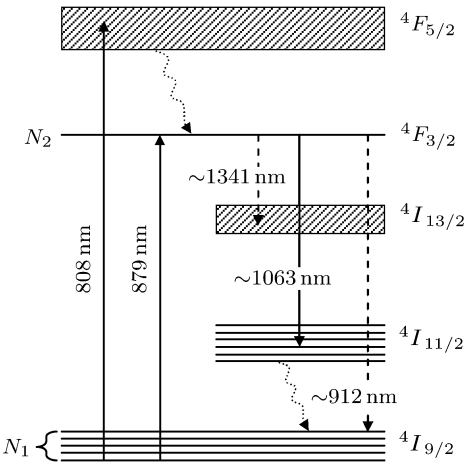


Fig.1. Energy-level scheme for Nd^{3+} in Nd^{3+}:$GdVO_4$ crystal.

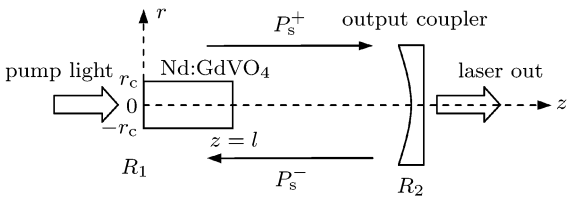


Fig.2. Schematic of an end-pumped Nd^{3+}:$GdVO_4$ laser.

The schematic of an end-pumped Nd^{3+}:$GdVO_4$ laser is shown in Fig.2. The z-axis is the optical axis with its origin at the front facet of the crystal. In our model, we assume that the transverse modes of the pump and the laser beams are TEM_{00} Gaussian beams with a negligible diffraction in a gain medium, which present a rotational symmetry about the z-axis. So we adopt cylindrical coordinates (r, z) where the variable r is the transverse radial coordinate. Possible effects of spatial hole-burning will be neglected, and it is assumed that the pump light passes through the laser medium only once. For TEM_{00} Gaussian beams, the pump and the laser intensities can be written as

$$I_p(r,z) = \frac{2P_p(z)}{\pi\omega_p^2(z)} e^{-\frac{2r^2}{\omega_p^2(z)}} \quad (1)$$

and

$$I_s(r,z) = \frac{2\left[P_s^+(z) + P_s^-(z)\right]}{\pi\omega_s^2(z)} e^{-\frac{2r^2}{\omega_s^2(z)}}, \quad (2)$$

where $P_p(z)$ is the pump power at location z in the cavity, $P_s^{\pm}(z)$ are the laser powers at z, in which superscripts + and – represent the forward and the backward directions respectively; $\omega_p(z)$ and $\omega_s(z)$ are the radii of the pump and the laser beams at z, respectively, and they are defined in the same form

$$\omega_i(z) = \omega_{i0}\left\{1 + \left[\frac{\lambda_i(z-z_0)}{\pi n_i \omega_{i0}^2}\right]^2\right\}^{1/2}, \quad (3)$$

where i=p, s; ω_{i0} is the beam radius at waist $z = z_0$; λ_i is the wavelength; n_i is the refractive index of the crystal at the corresponding wavelength. Generally, when the crystal is several millimetres in thickness, the variation of the beam radius in the crystal is quite small so that the approximation, $\omega_i(z) \approx \omega_{i0}$, adopted in our model is reasonable.

2.1. Direct pumping at 879 nm

In a direct pumping scheme, Nd^{3+} ions are excited to the upper laser level $^4F_{3/2}$ directly from the lowest Stark component of the ground manifold $^4I_{9/2}$. By using the Judd–Ofelt theory[17,18] with the phenomenological spectral parameters of Nd^{3+}:$GdVO_4$[19] as well as the nonradiative relaxation theory with the nonradiative parameters of YVO_4,[20] the lifetime of the lower laser level $^4I_{11/2}$ of Nd^{3+} in $GdVO_4$ has been calculated by us to be only about 600–900 ps. This lifetime is so short that the ions in $^4I_{11/2}$ rapidly relax to the ground state. So for the four-level system, Nd^{3+} ions can be considered to populate only in the ground manifold $^4I_{9/2}$ and the upper laser level $^4F_{3/2}$, of which the population densities are denoted as N_1 and N_2, respectively. The space-dependent steady state rate equations can be written as

$$\frac{dN_2}{dt} = N_1 W_{12} - N_2 W_{21} - N_2 R_{em} - \frac{N_2}{\tau} = 0, \quad (4)$$

and

$$N_1 + N_2 = N_0, \tag{5}$$

where N_0 is the total Nd^{3+}-doped concentration, τ is the lifetime of $^4F_{3/2}$, W_{12} and W_{21} are the stimulated absorption and emission transition rates at a pump wavelength λ_p, R_{em} is the stimulated emission transition rate at a laser wavelength λ_s, they are expressed as

$$W_{12} = \frac{I_p(r,z)\sigma_{abs}}{h\nu_p}, \tag{6}$$

$$W_{21} = \frac{I_p(r,z)\sigma_{ep}}{h\nu_p}, \tag{7}$$

and

$$R_{em} = \frac{I_s(r,z)\sigma_{em}}{h\nu_s}, \tag{8}$$

with σ_{abs} and σ_{ep} being the effective absorption and the effective emission cross sections at λ_p respectively, σ_{em} the effective emission cross section at λ_s, and $h\nu_{p,s}$ the photon energies at $\lambda_{p,s}$.

The propagation equation for the pump beam is

$$\frac{dP_p(z)}{dz} = -P_p(z)\int_0^{r_c}(N_1\sigma_{abs} - N_2\sigma_{ep}) \times \varphi_p(r,z)2\pi r dr - \delta_p P_p(z). \tag{9}$$

The propagation equations for a bidirectionally propagating laser beam are

$$\frac{dP_s^{\pm}(z)}{dz} = \pm P_s^{\pm}(z)\int_0^{r_c} N_2\sigma_{em}\varphi_s(r,z)2\pi r dr \mp \delta_s P_s^{\pm}(z), \tag{10}$$

where r_c is the transverse size of the laser medium, δ_p and δ_s are the background losses for the pump and the laser beams respectively. And we assume that the losses exist only in the laser crystal and are taken as zero in an air cavity region. In the following calculations, $\delta_p = \delta_s = \delta$ is adopted. $\varphi_p(r,z)$ and $\varphi_s(r,z)$ are the Gaussian distribution functions for the pump and the laser beams respectively, and they are given by

$$\varphi_i(r,z) = \frac{2}{\pi\omega_i^2(z)}e^{-\frac{2r^2}{\omega_i^2(z)}} \approx \frac{2}{\pi\omega_{i0}^2}e^{-\frac{2r^2}{\omega_{i0}^2}}, \tag{11}$$

where i=p, s. And from Eq.(10), a simple relationship can be derived

$$P_s^+(z)\cdot P_s^-(z) = C, \tag{12}$$

where C is the constant that is independent of the spatial coordinates r and z.

Boundary conditions are required for the solutions of Eqs.(9) and (10):

$$P_p(z=0) = P_{in}, \tag{13}$$

$$P_s^+(z=0) = R_1 P_s^-(z=0), \tag{14}$$

and

$$P_s^-(z=l) = R_2 P_s^+(z=l), \tag{15}$$

where P_{in} is the pump power incident upon the front facet of the laser crystal, l is the crystal length, R_1 and R_2 are the reflectivities of the front facet of the crystal and the output coupler at 1063 nm, respectively. From expressions (12) and (14), we have

$$P_s^-(z) = \frac{[P_s^+(z=0)]^2}{R_1 P_s^+(z)}, \tag{16}$$

which can be substituted into expression (2) to eliminate the $P_s^-(z)$ term. From expressions (12), (14) and (15), boundary condition can be rewritten as

$$P_s^+(z=0) = P_s^+(z=l)\sqrt{R_1 R_2}. \tag{17}$$

In the calculations, we divide the crystal into quite a number of slices along the z-axis, and the size of each slice dz is small enough such that the assumption holds true that the pump power $P_p(z)$ and the laser power $P_s^+(z)$ are constant in each slice. If the powers $P_p(z)$ and $P_s^+(z)$ at location z are known, we can obtain the population densities at (r,z) by solving the steady state rate equations, and then the powers at next location $z' = z + dz$, $P_p(z')$ and $P_s^+(z')$, can be determined by solving the propagation equations with the fourth-order Runge–Kutta method. According to this principle, with an initial value for laser power $P_s^+(z=0)$ assumed, the laser power $P_s^+(z=l)$ at location l can be obtained eventually. If the relationship between $P_s^+(z=0)$ and $P_s^+(z=l)$ accords with the boundary condition (17), the value of $P_s^+(z=l)(1-R_2)$ is the output power. Otherwise we will change the initial laser power $P_s^+(z=0)$ until the boundary condition is achieved.

2.2. Indirect pumping at 808 nm

In an indirect pumping scheme, Nd^{3+} ions are excited to the $^4F_{5/2}$ level and then populated to the $^4F_{3/2}$ level through a very fast nonradiative process. The theory of indirect pumping is the same as that of direct pumping except for the rate equation for N_2 and the propagation equation for pump beam because of the absence of the stimulated emission at the pump wavelength. They are given by

$$\frac{dN_2}{dt} = N_1 W_{12} - N_2 R_{em} - \frac{N_2}{\tau} = 0, \tag{18}$$

$$\frac{\mathrm{d}P_{\mathrm{p}}(z)}{\mathrm{d}z} = -P_{\mathrm{p}}(z)\int_0^{r_{\mathrm{c}}} N_1\sigma_{\mathrm{abs}}\varphi_{\mathrm{p}}(r,z)2\pi r\mathrm{d}r - \delta_{\mathrm{p}}P_{\mathrm{p}}(z). \quad (19)$$

2.3. Threshold

In most cases it is necessary to calculate the threshold pump power. The round-trip threshold gain G_{th}, namely the round-trip loss of the cavity, is usually given by

$$G_{\mathrm{th}} = \ln\frac{1}{R_1R_2} + 2\delta l. \quad (20)$$

In our model the round-trip gain G for a laser beam can be determined by

$$G = 2\int_0^l\int_0^{r_{\mathrm{c}}} N_2(r,z)\sigma_{\mathrm{em}}\varphi_{\mathrm{s}}(r,z)2\pi r\mathrm{d}r\mathrm{d}z. \quad (21)$$

In threshold calculations, $I_{\mathrm{s}}(r,z) = 0$. Make P_{in} variable, and the value of P_{in} for $G = G_{\mathrm{th}}$ will correspond to the threshold.

3. Comparison with experimental results

Lupei *et al*[11] have obtained a highly-efficient 1063-nm CW laser emission from in Nd^{3+}:$GdVO_4$ longitudinally pumped by Ti:sapphire 808 and 879 nm lasers, respectively. In this section we compare the numerical results of our theoretical model with their experimental results. The parameters used for numerical calculations are cited from Ref.[11] and listed in Table 1. It should be noted that the background loss

Table 1. Parameters used for numerical simulations.

parameters	values
N_0	6.049×10^{19} cm^{-3} (0.5 at%)
l	3 mm
R_1	99.8%
R_2	97%, 95%, 80%
δ	1.3 m^{-1}
ω_{p0}	25 μm
ω_{s0}	90 μm
r_{c}	1.5 mm

δ is the deduced value based on $2\delta l = 0.8\%$.[11] Other parameters used for simulations are as follows: $\tau = 92\,\mu$s,[9] $\sigma_{\mathrm{em}} = 10.3\times10^{-19}$ cm^2,[9] $\sigma_{\mathrm{ep}} = 2.5\times10^{-19}$ cm^2,[21] and $\sigma_{\mathrm{abs}}(808\,\mathrm{nm}) = 5.36\times10^{-19}$ cm^2,[2] and $\sigma_{\mathrm{abs}}(879\,\mathrm{nm}) = 2.7\times10^{-19}$ cm^2.[11]

The plots of the calculated laser output power at 1063 nm versus incident pump power under direct and indirect pumping are shown in Figs.3 and 4, respectively, together with a comparison with the experimental results. It can be seen that the theoretical and the experimental data are in rather good agreement with each other. Under the direct pumping and the indirect pumping, the slope efficiencies are quite high with transmission T of the output coupler varying from 3% to 20%. Under direct pumping at 879 nm and $T = 20\%$, the calculated slope efficiency for the incident pump power η_{s} reaches up to 78.8%, and the output power reaches 1.39W for a 1.8W incident power, corresponding to an optical-to-optical efficiency η_{o} of 77.2%; while in the case of 1.8W indirect pumping at 808 nm, η_{s} drops to 73.4% and η_o to 72.2%. Compared with the indirect pumping, the direct pumping enhances the quantum defect ratio between the pump and laser wavelengths,[22] so the slope efficiency for the absorbed pump power under direct pumping is always higher than under indirect pumping. But when the slope efficiency for the incident pump power is concerned about, direct pumping is not always better than indirect pumping.[23] In the present laser conditions the slope efficiency for the incident pump power under direct pumping is higher than under indirect pumping by comparing Fig.3 with Fig.4, so in the following calculations we will adopt the direct pumping scheme.

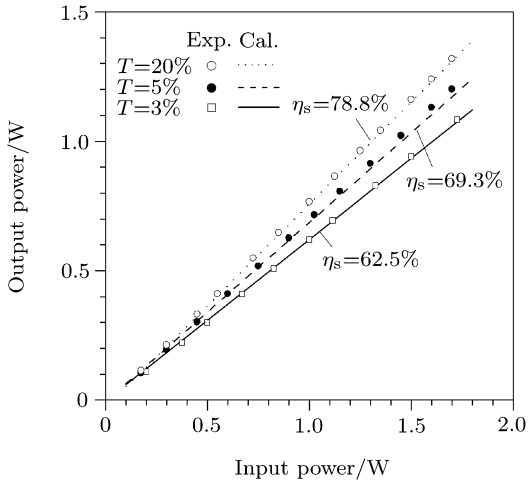


Fig.3. Laser output power versus incident pump power under direct pumping, where theoretical and experimental results are shown by lines and spots respectively.

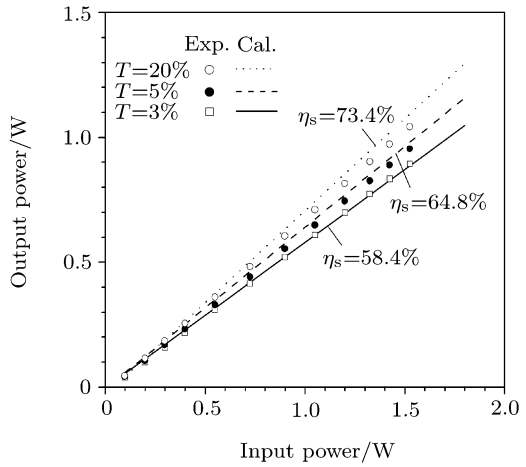


Fig.4. Laser output power versus incident pump power under indirect pumping, where theoretical and experimental results are shown by lines and spots respectively.

4. Optimization of output power

The agreement between the calculated and the published experimental results enables us to verify the theoretical model presented in this paper for an end-pumped 1063-nm CW Nd^{3+}:$GdVO_4$ laser. In this section, therefore, we use this model to discuss the parameters including the reflectivity of output coupler, the spot size of laser beam, and the crystal length for optimizing the laser performance. The parameters used in the following calculations are the same as those in Section 3 unless otherwise stated.

4.1. Reflectivity of the output coupler

Figure 5 shows the curves for laser output power versus the reflectivity R_2 of the output coupler for different incident pump powers. All the curves decrease obviously in the high- and the low-reflectivity regions. It can be seen that there exists an optimal value of R_2 for each incident power which can maximize the output power, and this optimum shifts to lower values with the increase of the incident power. Figure 6 shows the optimal reflectivity $R_{2\,\mathrm{opt}}$ as a function of the incident power. In Ref.[11] the maximal incident power was 1.7W and the values of R_2: 97%, 95% and 80%, were used respectively. The laser had a best output for R_2 = 80%, which is close to our calculated $R_{2\,\mathrm{opt}}$ of 76%. Here, although the incident power reaches 20W, the aim of the present paper is to find out approximate relationships between various values of laser parameters, so the thermal effect resulting from the high power is not taken into account. We have investigated the pump threshold versus the reflectivity as shown in Fig.7. A larger value of R_2 leads to a lower threshold. For R_2 = 80% a calculated threshold of 38mW is consistent with the experimental result 31mW.[11] In the following calculations, the value of R_2 is 80%.

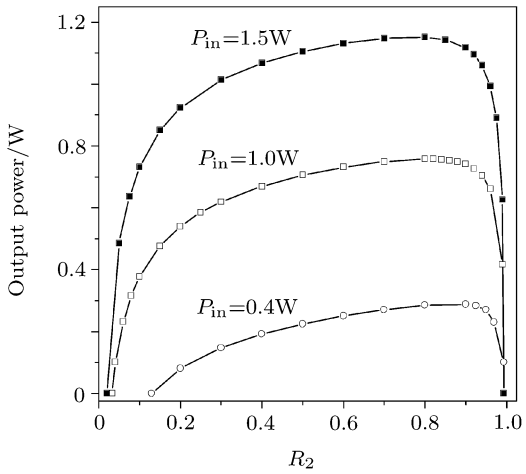


Fig.5. Curves for laser output power versus reflectivity R_2 of the output coupler for different incident pump powers.

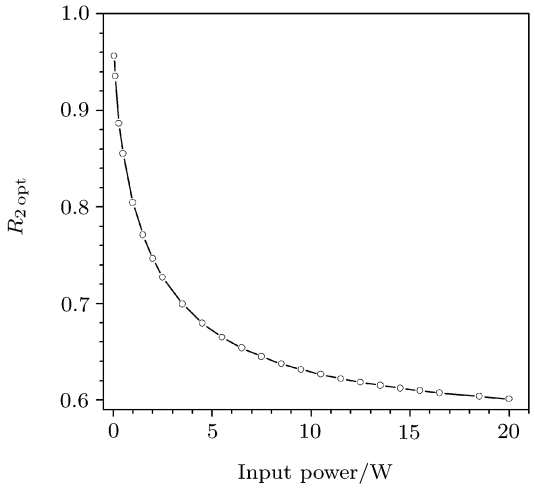


Fig.6. Optimal reflectivity $R_{2\,\mathrm{opt}}$ of the output coupler as a function of the incident pump power.

4.2. Spot size of the laser beam

The spot sizes of both the pump and the laser beams are important parameters because they determine the spatial overlap between the two beams in an active medium, and hence they can influence the threshold, slope efficiency and laser output power. In this section, we make the spot size of the pump beam unchangeable (ω_{p0}=25 μm) and define the spot size ratio $\alpha = \omega_{\mathrm{s0}}/\omega_{\mathrm{p0}}$, and then investigate the influence of α on the laser performance.

Figure 8 illustrates the behaviours of the slope efficiency and threshold each as a function of α. The slope efficiency rapidly increases with α as $\alpha < 0.9$, and then this trend sharply diminishes with the slope efficiency approaching a constant of 79% as α exceeds 0.9. This effect can be interpreted as follows. As the laser spot size becomes larger, the laser mode volume has a larger overlap with the pump volume, leading to a more efficient extraction of the pump energy and hence a higher slope efficiency. However, once the size of the laser beam is larger than that of the pump beam, the activated area will be completely covered by the laser mode. And the pump energy can be maximally converted into laser energy, and thus the slope efficiency becomes approximately independent of the spot size of the laser beam. As for the threshold, it increases with α, and by simple calculation one can find that the threshold is linearly varied with α^2, which accords with the analytical result given in Refs.[12] and [13].

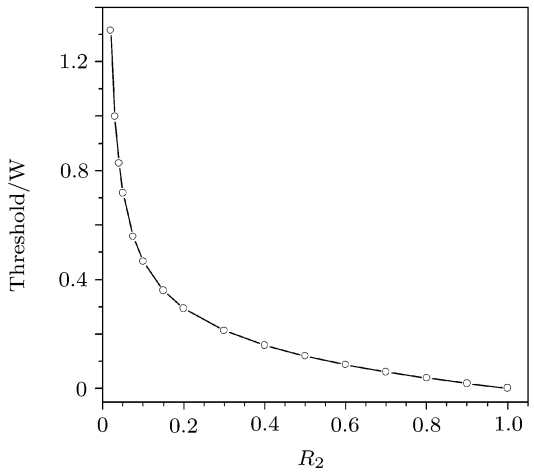


Fig.7. Pump threshold versus reflectivity R_2 of the output coupler.

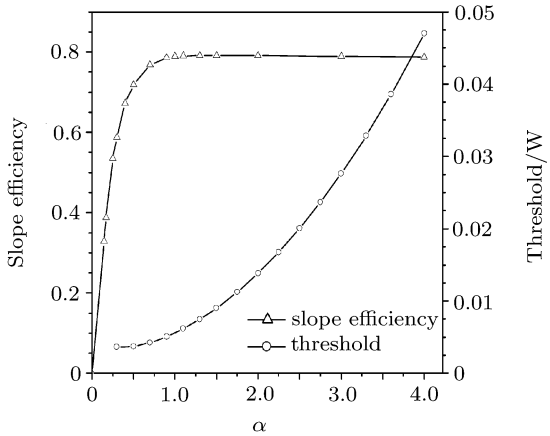


Fig.8. Slope efficiency and threshold each as a function of the spot size ratio α.

Figure 9 shows the curves for laser output power versus α for several incident pump powers, from which we can more intuitively see the influence of α on the laser performance. For each incident pump power, the output power is initially a rapidly increasing function of α, which can be interpreted by the rapid increase of the slope efficiency in Fig.8. There exists an optimal ratio $\alpha_{\rm opt}$ to maximize the output power. When it is larger than the optimum, α gives rise to only a minor decrease in output power. This fact is consistent with the phenomenon revealed by the dependences of the slope efficiency and the threshold on α (see Fig.8).

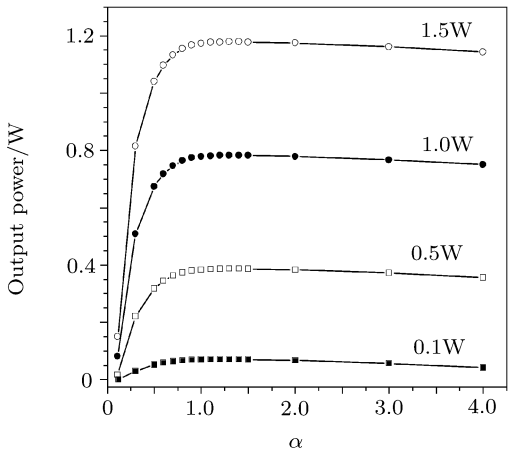


Fig.9. Curves for laser output power versus spot size ratio α for several incident pump powers.

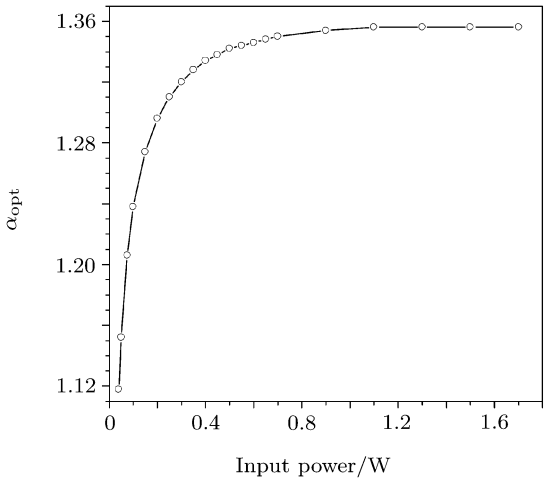


Fig.10. Optimal spot size ratio $\alpha_{\rm opt}$ as a function of the incident pump power.

The optimal ratio $\alpha_{\rm opt}$ is an ascending function of the incident pump power as shown in Fig.10. However, this kind of ascending trend diminishes and eventually $\alpha_{\rm opt}$ tends to a constant independent of the incident power. This effect is obviously related to the dependences of the slope efficiency and the threshold on the

ratio α as shown in Fig.8. In the present laser system α_{opt} tends to 1.356, namely the optimal spot size of the laser beam is 34 μm under a stronger pump power. By utilizing Fig.10 it is easy to determine the optimal laser spot size for a given pump power, which is helpful for obtaining a guideline for designing the laser resonator.

4.3. Length of the crystal

Figure 11 shows the curves for laser output power as a function of the crystal length for different incident pump powers. In the calculation the experimental data $\omega_{p0} = 25\,\mu$m and $\omega_{s0} = 90\,\mu$m have been used, namely $\alpha = 3.6$. The curves exhibit that their shapes are the same on the whole. When the crystal length is very short, the output power increases steeply with the increase of the length, during which the pump power is not fully absorbed. The output power reaches a maximum corresponding to an optimal crystal length, which occurs when nearly all the pump power is absorbed. From calculations we find that the pump power is absorbed over 99% at the optimal length. The output power has a nearly linear decrease at the crystal lengths in excess of the optimum. Relative to the optimal length, the extended region of the crystal cannot be sufficiently activated to establish population inversion by the residual pump energy, which just results in the reabsorption of the signal light.

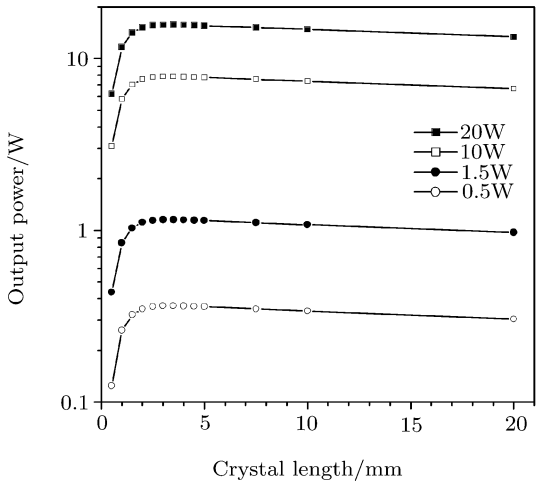


Fig.11. Curves for laser output power as a function of the crystal length for several incident pump powers.

In calculation for Fig.11, the spot size ratio α is fixed at 3.6. In fact, the optimal crystal length l_{opt} is related to α as can be seen from Fig.12 which shows that the value of l_{opt} has a minimum when α is near to the unity. It can also be seen that l_{opt} is 3.32 mm as α is 3.6, so it is basically appropriate to employ the Nd^{3+}:$GdVO_4$ crystal of a 3 mm in length in the lasing experiment by Lupei *et al.*[11]

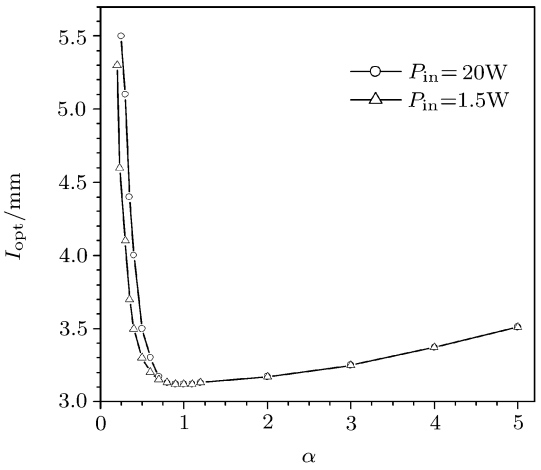


Fig.12. Curves for optimal crystal length l_{opt} versus spot size ratio α.

In addition, we find that for a given α the optimal length l_{opt} seems to be independent of the incident pump power P_{in} for Nd^{3+}:$GdVO_4$ crystal, which is different from the general cases, i.e. l_{opt} shifts to larger values with the increase of P_{in}. As shown in Fig.11, the optimal lengths have the same value of 3.32 mm for pump powers: 0.5, 1.5, 10 and 20W. Even when P_{in} increases up to thousands of watts, the calculated optimum is still 3.32 mm. The reason for this is that in the model we neglect the population of the lower laser level $^4I_{11/2}$ due to its very short lifetime. In this case, the population of the ground state is hardly influenced by the increase of P_{in} provided that the lasing action is intense enough, so the crystal may keep rather strong absorption for pump beam and l_{opt} does not lengthen with P_{in}. But when the effect of $^4I_{11/2}$ population is taken into account and P_{in} is high enough, $^4I_{11/2}$ will have a considerable population though it has a very short lifetime, which will decrease the pump beam absorption, and hence a longer optimal crystal length is required for a higher incident pump power. To verify this explanation, we consider the population effect of $^4I_{11/2}$ by assuming its lifetime to be 1 ns, and here the calculated l_{opt} is found to be 3.42 mm for an incident power of 1000W and 3.78 mm for 5000W by using our model. For pump powers under several hundred watts, however, the l_{opt} value almost maintains invariable. So when the incident pump power is very high,

it is necessary to consider the population of the lower laser level $^4I_{11/2}$.

More investigations on the diode-pumped CW Nd^{3+}:$GdVO_4$ lasers have been carried out in recent years.[7−10] If the realistic beam mode of the pumping diode laser (not TEM_{00} Gaussian because of the poor quality of diode laser beam) is taken into account, our model will still hold for the case of diode-pumped CW Nd^{3+}:$GdVO_4$ lasers.

5. Conclusions

A theoretical model to simulate an end-pumped CW Nd^{3+}:$GdVO_4$ laser at 1063 nm has been developed. Its essence is to use propagation equations to demonstrate the spatial evolutions of the pump and the laser powers in the cavity, and this model has been verified by the experimental data for a Ti:sapphire-pumped Nd^{3+}:$GdVO_4$ laser published in the literature. By using the model we have investigated the influences of the laser parameters on the laser performance, such as the reflectivity of output coupler, the spot size of laser beam as well as the crystal length. The optimal parameter values have been determined. For example, the optimal reflectivity of output coupler is around 80% when pump power is less than 2W; the optimal spot size ratio between the pump and the laser beams is about 1.356 for a 3 mm long crystal and the optimal crystal length is about 3.32 mm for a spot size ratio of 3.6. The model presented in this paper could be applied to the study on various end-pumped CW laser emissions.

Acknowledgment

The authors would like to thank Professor Lupei V and Dr Pavel N (Institute of Atomic Physics, Solid State Quantum Electronics Laboratory, Bucharest, R-76900 Romania) for providing their experimental laser parameters and some helpful discussions.

References

[1] Zagumennyi A I, Ostroumov V G, Shcherbakov I A, Jensen T, Meyn J P and Huber G 1992 *Sov. J. Quantum Electron.* **22** 1071
[2] Czeranowsky C, Schmidt M, Heumann E, Huber G, Kutovoi S and Zavartsev Y 2002 *Opt. Commun.* **205** 361
[3] Jensen T, Ostroumov V G, Meyn J P, Huber G, Zagumennyi A I and Shcherbakov I A 1994 *Appl. Phys.* B **58** 373
[4] Studenikin P A, Zagumennyi A I, Zavartsev Y D, Popov P A and Shcherbakov I A 1995 *Quantum Electron.* **25** 1162
[5] Li P X, Li D H, Li C Y and Zhang Z G 2004 *Chin. Phys.* **13** 1689
[6] Zhang Y P, Zheng Y, Zhang H Y, Wang P and Yao J Q 2006 *Chin. Phys.* **15** 2018
[7] Liu J, Shao Z, Zhang H, Meng X, Zhu L and Jiang M 1999 *Appl. Phys.* B **69** 241
[8] Yang J, Liu J and He J 2005 *Laser Phys. Lett.* **2** 171
[9] Pavel N and Taira T 2006 *Opt. Commun.* **260** 271
[10] Qin L J, Meng X L, Du C L, Shao Z S, Zhu L, Xu B C and Zhang H J 2002 *Cryst. Res. Technol.* **37** 913
[11] Lupei V, Pavel N, Sato Y and Taira T 2003 *Opt. Lett.* **28** 2366
[12] Fan T Y and Byer R L 1987 *IEEE J. Quantum Electron.* **23** 605
[13] Risk W P 1988 *J. Opt. Soc. Am.* B **5** 1412
[14] Chang J, Wang Q P, Zhang X Y, Liu Z J and Liu Z J 2005 *Opt. Express* **13** 3902
[15] Chang J, Wang Q P, Peng G D, Zhang X Y, Liu Z J, Ding S H, Liu Z J, Zhang S S and Wang G T 2006 *Opt. Express* **14** 8535
[16] Chang J, Wang Q P and Peng G D 2006 *Opt. Mater.* **28** 1088
[17] Judd B R 1962 *Phys. Rev.* **127** 750
[18] Ofelt G S 1962 *J. Chem. Phys.* **37** 511
[19] Jiang H D, Zhang H J, Wang J Y, Xia H R, Hu X B, Teng B and Zhang C Q 2001 *Opt. Commun.* **198** 447
[20] Ermeneux F S, Goutaudier C, Moncorge R, Sun Y, Cone R L, Zannoni E, Cavalli E and Bettinelli M 2000 *Phys. Rev.* B **61** 3915
[21] Herault E, Balembois F and Georges P 2006 *Opt. Lett.* **31** 2731
[22] Clarkson W A 2001 *J. Phys.* D **34** 2381
[23] Huang Z Y, Huang Y D, Chen Y J and Luo Z D 2005 *J. Opt. Soc. Am.* B **22** 2564